RSC Advances

PAPER

View Article Online
View Journal | View Issue

Check for updates

Cite this: *RSC Adv.*, 2020, **10**, 42971

Material balance in the O_2 electrode of Li–O_2 cells with a porous carbon electrode and TEGDME-based electrolytes†

Makoto Ue, *[a] Hitoshi Asahina, [ab] Shoichi Matsuda [ab] and Kohei Uosaki [ab]

This work figures out the material balance of the reactions occurring in the O_2 electrode of a Li–O_2 cell, where a Ketjenblack-based porous carbon electrode comes into contact with a tetraethylene glycol dimethyl ether (TEGDME)-based electrolyte under more practical conditions of less electrolyte amount and high areal capacity. The ratio of electrolyte weight to cell capacity (E/C, g A h^{-1}) is a good parameter to correlate with cycle life. Only 5 cycles were obtained at an areal capacity of 4 mA h cm^{-2} (E/C = 10) and a discharge/charge current density of 0.4 mA cm^{-2}, which corresponds to the energy density of 170 W h kg^{-1} at a complete cell level. When the areal capacity was decreased to half (E/C = 20) by setting a current density at 0.2 mA cm^{-2}, the cycle life was extended to 18 cycles. However, the total electric charge consumed for parasitic reactions was 35 and 59% at the first and the third cycle, respectively. This surprisingly large amount of parasitic reactions was suppressed by half using redox mediators at 0.4 mA cm^{-2} while keeping a similar cycle life. Based on by-product distribution, we will propose possible mechanisms of TEGDME decomposition and report a water breathing behavior, where H_2O is produced during charge and consumed during discharge.

Received 16th September 2020
Accepted 11th November 2020

DOI: 10.1039/d0ra07924c

rsc.li/rsc-advances

Open Access Article. Published on 07 December 2020. Downloaded on 2/23/2026 11:56:04 AM.
This article is licensed under a Creative Commons Attribution-NonCommercial 3.0 Unported Licence.

Introduction

Electrochemical energy storage is a key technology in our modern society, and the Nobel Prize in Chemistry 2019 rewarded the development of the lithium-ion battery (LIB).[1,2] Although the energy density of the current LIB is approaching 300 W h kg^{-1}, this value is not sufficient for electric vehicles (EVs) with a driving range more than 500 km and an equivalent price with gasoline cars. These demands have energized the evolution of other alternative rechargeable batteries, so-called 'beyond LIB', which have a higher energy density over 500 W h kg^{-1}.[3] They are also now targeting the markets where mass is the critical factor above all, and considered as likely candidates for unmanned aerial vehicles (UAVs), which slowly charge their batteries during the day and discharge them overnight.

A potential candidate, the rechargeable nonaqueous Li–O_2 technology, was discovered by Abraham *et al.* in 1996,[4] although the history of Li–O_2 chemistry dates back to the 1960s.[5] The nonaqueous Li–O_2 batteries have garnered considerable research interest over the past decade due to their extremely high theoretical energy densities. For instance, it is calculated to be 3150 W h kg^{-1},[3] by multiplying an assumed operating voltage of 2.7 V by the specific capacity of 1168 A h kg^{-1} based on the reaction $2Li + O_2 = Li_2O_2$.

Although many studies including those in companies such as Samsung,[6,7] IBM,[8] Toyota[9] have been devoted to the discoveries of new materials and reaction mechanisms, the research activity on Li–O_2 technology seems to be decreasing around 2015 from the viewpoint of the number of publications.[10] Because the nonaqueous Li–O_2 batteries are still in their infancy due to numerous problems,[11,12] there is no report, which actually attained the energy density of 500 W h kg^{-1} in a complete cell level as a rechargeable battery.[6,10] The present authors also have tried to fabricate a Li–O_2 cell for the application to a high altitude platform station (HAPS) and found it difficult to achieve both satisfactory energy density and cycle life. Except a few works,[6,7,13] almost all studies reported so far included too much excess weight of electrolytes, which results in much lower energy densities than those of LIBs.[10] When the electrolyte amount is decreased to fulfill the energy density of 500 W h kg^{-1}, the cell cannot be cycled.

The electrolytes are the prime suspects for cell failure, and finding stable electrolytes remains as the most pressing scientific challenge.[14,15] Although a stable electrolyte has not been found yet, a combination of tetraethylene glycol dimethyl ether (TEGDME, tetraglyme) solvent and lithium bis(trifluoromethanesulfonyl)imide ($LiN(CF_3SO_2)_2$, LiTFSI) salt is the most popular electrolyte due to its relatively high stability, and various physicochemical properties such as electrolytic conductivity,[16–21] viscosity,[16,17,21] ion association degree,[18,20] Li^+

[a]*Center for Green Research on Energy and Environmental Materials, National Institute for Materials Science (NIMS), Japan. E-mail: macue01@gmail.com*

[b]*SoftBank-NIMS Advanced Technologies Development Center, 1-1 Namiki, Tsukuba, Ibaraki 305-0044, Japan*

† Electronic supplementary information (ESI) available. See DOI: 10.1039/d0ra07924c

Open Access Article. Published on 07 December 2020. Downloaded on 2/23/2026 11:56:04 AM.
This article is licensed under a Creative Commons Attribution-NonCommercial 3.0 Unported Licence.

transport number,[18,19,21] anodic stability,[18,21,22] freezing point,[18] boiling point,[16,21] vapor pressure,[16,21] oxygen solubility,[17,21] oxygen diffusion constant,[21] flammability,[18] contact angle,[16] have been reported in addition to cell performance.[13,16–23]

The discharge reaction is oxygen reduction reaction (ORR) taking place at the positive electrode, which generally uses porous carbon electrodes. It is believed that an oxygen molecule is reduced to form a superoxide radical anion ($O_2^{\bullet-}$) after extracting one electron from the carbon electrode. The resultant superoxide radical anion can coordinate with one Li^+ ion to form an intermediate product, lithium superoxide (LiO_2, eqn (1)). LiO_2 is not thermodynamically stable and would transiently convert to Li_2O_2 through either an electrochemical reaction (eqn (2)) and/or a chemical disproportionation reaction (eqn (3)). On the other hand, the charge reaction is oxygen evolution reaction (OER), where Li_2O_2 is oxidized to O_2 either by initial delithiation *via* $Li_{2-x}O_2$ or LiO_2 (a mirror process of eqn (2)) followed by the reaction (eqn (3)) and/or a direct two-electron electrochemical reaction without the formation of LiO_2 (eqn (4)).

$$O_2 + Li^+ + e^- \rightarrow LiO_2 \quad (1)$$

$$LiO_2 + Li^+ + e^- \rightarrow Li_2O_2 \quad (2)$$

$$2LiO_2 \rightarrow Li_2O_2 + O_2 \quad (3)$$

$$Li_2O_2 \rightarrow O_2 + 2Li^+ + 2e^- \quad (4)$$

The parasitic reactions have traditionally been ascribed to the reactions with reduced oxygen species ($O_2^{\bullet-}$ and O_2^{2-}), however, recent studies proved that singlet oxygen ($^1O_2$), which is partly generated by the superoxide disproportionation (eqn (3)), accounts for the majority of parasitic reaction by-products both on discharge and charge.[24] Many papers suggest that TEGDME decomposes in the carbon positive electrode during discharge and charge, however, it is only reported that the formation of Li_2O_2 on the first discharge was accompanied by the formation of Li_2CO_3, HCO_2Li, CH_3CO_2Li, polyethers/esters, CO_2, H_2O[25] and CH_3OH, $CH_3OCH_2CH_2OH$, $CH_3O(CH_2CH_2O)_2$-CH_3,[26] and the electrochemical decomposition of Li_2O_2 to O_2 on recharge was accompanied by more harsh decomposition with the similar by-products. If the TEGDME reacts with the superoxide radical anion, it can form new radicals, leading to by-products proposed by eqn (5).[25]

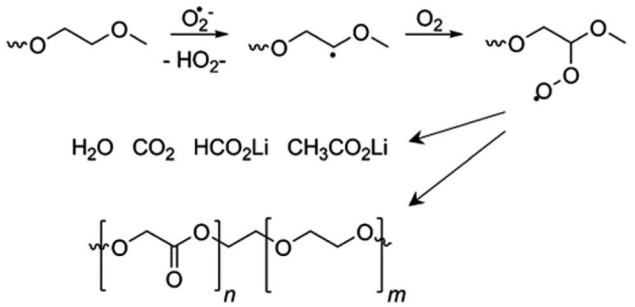

(5)

Furthermore, it is well known that coulombic efficiency (CE) of Li metal negative electrodes in nonaqueous electrolytes during cycling is very low due to the high reactive nature of Li metal, and most researchers use a thick Li foil, which can constantly offset Li loss during cycling and then mask poor cycling performance,[3,10] even in the case of Li–O_2 cells with TEGDME-based electrolytes.[27–29]

Therefore, it is especially important to quantify the decomposition reactions in a porous carbon positive electrode under more practical conditions of less electrolyte amount and high areal capacity without interference from Li metal negative electrode. We have examined reaction products in a porous carbon positive electrode by using a two-compartment cell design, where anode and cathode compartments were separated by a solid-state Li^+ conductor to eliminate possible interference from the reactions at Li metal negative electrode.[30] Because the monitoring the gas consumed/produced during the operation is nearly the only way to determine the CE of the O_2 electrode, we used on-line gas analysis as well as pressure change measurements[31] for understanding parasitic reactions coming from electrolyte decomposition.

Experimental methods

Materials

TEGDME (battery grade) was obtained from Japan Advanced Chemicals Ltd. and used as received. LiTFSI (Li battery grade) was obtained from Kishida Chemical Co., Ltd. Lithium nitrate ($LiNO_3$, 99.99% trace metals basis) and lithium bromide (LiBr, 99.995% trace metals basis) were obtained from Sigma-Aldrich Co., LLC. All lithium salts were dried at 120 °C under vacuum before being used. A lithium foil (200 μm thick) was obtained from The Honjo Chemical Corp. The porous carbon electrode is a proprietary self-standing sheet consisting of a Ketjenblack and a carbon fiber (250 μm thick, 7 mg cm^{-2}-carbon), whose pore size distribution is given in Fig. S1 in the ESI.† A solid-state Li^+ conductor sheet (LICGC-AG-01, 180 or 90 μm thick) was obtained from Ohara, Inc. and dried at 120 °C under vacuum before being used. A polyethylene membrane separator (20 μm thick) was obtained form W-Scope Corp. A stainless steel mesh (200 μm thick, 16.7 mm ϕ, aperture ratio 73%) was obtained from Hohsen Corp.

Electrolyte and electrode preparation

Two kinds of liquid electrolytes, (a) 1 M LiTFSI/TEGDME and (b) 0.5 M LiTFSI + 0.5 M $LiNO_3$ + 0.2 M LiBr/TEGDME were prepared in a glove box in an Ar atmosphere. Their water content was about 10 ppm by the Nittoseiko Karl Fischer Moisture Meter CA-31. The densities of electrolytes (a) and (b) were 1.16 and 1.12 g cm^{-3} at 25 °C by the Anton Paar Lovis 2000 ME rolling-ball viscometer, respectively.

The proprietary porous carbon sheet was cut into a disc (16 mm ϕ) and dried at 120 °C under vacuum for 12 hours. Then, 80 μl of the electrolyte was impregnated into the porous carbon electrode at 40 °C under vacuum and the extra

 This journal is © The Royal Society of Chemistry 2020

Open Access Article. Published on 07 December 2020. Downloaded on 2/23/2026 11:56:04 AM.
This article is licensed under a Creative Commons Attribution-NonCommercial 3.0 Unported Licence.

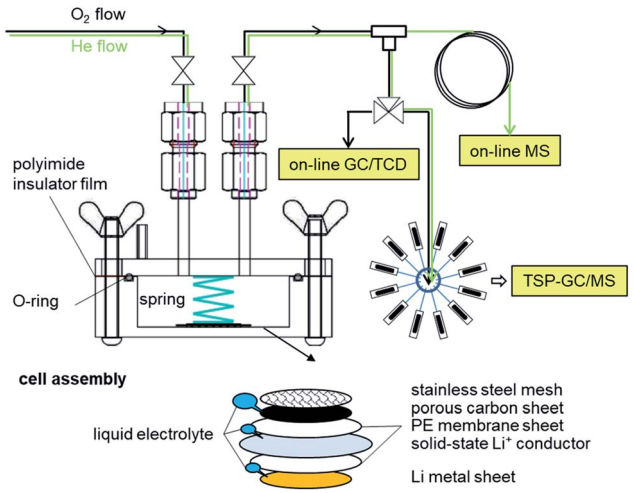

Fig. 1 A Li–O_2 two-compartment test cell and characterization tools for evolved gases.

electrolyte was wiped off by a filtration paper. The remained electrolyte in the porous carbon electrode was 60 μl.

Cell assembly

A custom-made test cell (stainless steel, inner diameter: 45 mm ϕ, depth: 15 mm) equipped with a gas inlet and outlet was assembled in a dry air atmosphere by stacking a Li metal electrode (200 μm thick, 16 mm ϕ), a polyethylene membrane (20 μm thick, 19.5 mm ϕ), a solid-state Li^+ conductor (180 or 90 μm thick, 22 mm ϕ), a polyethylene membrane (20 μm thick, 19.5 mm ϕ), a porous carbon electrode (250 μm thick, 16 mm ϕ, 7 mg cm^{-2}-carbon) impregnated with a liquid electrolyte (30 μl cm^{-2}), and a stainless steel mesh (200 μm thick, 16.7 mm ϕ) as shown in Fig. 1. Each 10 μl of the liquid electrolyte was added onto Li metal and the solid-state Li^+ conductor during assembling. The solid-state Li^+ conductor was sandwiched with a pair of polyethylene membranes to secure good contact between the electrodes and the solid-state Li^+ conductor. 35 kPa of pressure was applied to the cell assembly by a spring coil as shown in Fig. 1. After purged with O_2 flow (dew point below −70 °C) at 2 ml min^{-1} for 20 minutes, the cell was rested for 2 hours before electrochemical measurements.

Electrochemical measurements

The discharge/charge cycling tests were carried out by the Electrofield EF-7100P under O_2 flow (2 ml min^{-1}) at 0.2 or 0.4 mA cm^{-2} for 10 hours at ambient temperature followed by the resting time for 2 hours at each interval between discharge and charge.

Characterization methods

Continuous on-line gas chromatography analysis was carried out at three minutes interval by the Agilent 490 Micro GC system with a thermal conductivity detector (TCD), and Molesieve 5A and PoraPLOT Q columns.

On-line mass spectroscopy analysis was carried out by the Canon Anelva Quadrupole Mass Spectrometer M-401GA-DM. After discharge, the remaining O_2 in the cell was flushed out for 3 minutes by switching the inlet gas to He (50 ml min^{-1}), and then He flow was set to 5 ml min^{-1}. A part of the outlet gas was introduced through a capillary tube (internal diameter: 0.05 mm ϕ, length: 2 m) into MS to analyze the evolved gases during charge as shown in Fig. 1.

The decomposition products in gas phase were adsorbed by seven pieces of Agilent J&W HP-PLOT Q columns (inner diameter: 0.53 mm ϕ, length: 20 mm) packed parallel in a 1/8″ stainless tube cartridge every one hour. Each sample cartridge was set inside a thermal separation probe (TSP), and the desorbed gases at 250 °C were analyzed by the Agilent 5977C GC/MSD system equipped with a VF-WAXms column.

The decomposition products in liquid phase was analyzed by liquid chromatography analysis by the Waters Acquity H-class Ultra High Pressure Liquid Chromatography (UPLC) system coupled with a HSS T3 column and a Xevo G2-S QTof mass spectrometer.

The consumed/produced O_2 was estimated by ideal gas law from the pressure change in the closed cell (internal volume: 25 ml) equipped with a pressure sensor, Keyence AP44. After filling O_2 of about 0.13 MPa, the pressure change was monitored during cycling at 22 ± 0.1 °C.

Results and discussion

Discharge/charge behavior of a Li–O_2 two-compartment cell

The purpose of this work is to figure out the material balance of the reaction occurring in a Ketjenblack-based porous carbon positive electrode of a Li–O_2 cell with 1 M LiTFSI/TEGDME electrolyte under more practical conditions of less electrolyte amount and high areal capacity. The used porous carbon electrode has large pore volume in mesopore region as shown in Fig. S1 in the ESI.† A custom-made two-compartment test cell shown in Fig. 1 was used to examine decomposition products. Because the carbon positive electrode is separated from the Li metal negative electrode by a solid-state Li^+ conductor, it is possible to eliminate interference from the reactions at the negative electrode.

Most researchers have not been concerned about the amounts of Li metal electrode and liquid electrolyte, when they determined cycle life of Li–O_2 cells, even though these amounts are the important factors to determine not only energy density but also cycle life. Almost all studies so far have been carried out using a thick Li foil (100–500 μm thick). Because the equivalent weight of Li and graphite are 3860 and 372 mA h g^{-1}, respectively, the capacity ratio of negative to positive electrodes (N/P ratio) should be at least less than 3860/372 ≒ 10 to keep the advantage over graphite electrodes. When the areal capacity of the Li metal anode is set to 4 mA h cm^{-2} (our standard experiment condition for the positive electrode), the thickness of the Li metal is calculated to be about 20 μm.

On the other hand, the electrolyte amount has a more significant influence on the energy density than the Li metal thickness owing to the larger mass density of the electrolyte

Open Access Article. Published on 07 December 2020. Downloaded on 2/23/2026 11:56:04 AM.
This article is licensed under a Creative Commons Attribution-NonCommercial 3.0 Unported Licence.

Table 1 Cell parameters and cycle life of Li–O_2 cells with 1 M LiTFSI/TEGDME in recent studies

Capacity (mA h cm^{-2})	Electrolyte amount (mg cm^{-2})	Carbon loading (mg cm^{-2})	E/C (g A h^{-1})	Specific capacity (mA h g^{-1}-carbon)	Li thickness (μm)	Cycle life (@mA cm^{-2})	Ref.
4	41	7	10	571	200	5 (0.4)	This work
2	41	7	20	286	200	18 (0.2)	This work
13.5	41	14	3	938	160	2 (0.15)	13
9.7	41	14	4	679	160	3 (0.15)	13
6.7	41	14	6	467	160	4 (0.15)	13
3.4	41	14	12	236	160	8 (0.15)	13
1	50[a]	1	50	1000	160	40 (0.1)	13
0.3	51	0.6	171	500	?	20 (0.2)	17
0.4	50[a,b]	0.8	125	500	?	250 (0.08)	18
0.25	50[a]	0.5	200	500	?	40 (0.125)	19
0.5	50[a]	1	100	500	500	15 (0.2)	20
1	50[a]	1	50	1000	450	40 (0.2)	21
0.5	50[a]	0.5	100	1000	300	10 (0.1)	22
1.25	189	1	151	1250	?	2 (0.075)	23

[a] An assumed amount for coin or Swagelok-type cells. [b] 0.4 M.

(1.16 g cm^{-3}) than that of Li metal (0.53 g cm^{-3}). The ratio of the electrolyte volume to the total pore volume of cell components is an important parameter, however, the ratio of electrolyte weight to cell capacity (E/C, g A h^{-1}) is empirically used to represent the electrolyte amount in LIBs.[10] The E/C ratio in our experiments is 10 g A h^{-1}, which is much smaller than those of previous studies (E/C ≥ 50 g A h^{-1}, except ref. 13) as listed in Table 1. Only 5 cycles were obtained at 0.4 mA cm^{-2} (cut off: 4 mA h cm^{-2}, 571 mA h g^{-1}-carbon) as shown in Fig. 2a. While stable 18 cycles were achieved when the areal capacity was decreased to half by setting a current density at 0.2 mA cm^{-2} as shown in Fig. 2b, where E/C is 20 g A h^{-1}.

Our experimental conditions shown in the first and second lines in Table 1, correspond to energy densities of about 170 and 90 W h kg^{-1}, respectively, for a complete cell without a solid-state Li^+ conductor based on our simulation (N/P = 2.5).[10] On the other hand, those of previous studies (except ref. 13) in Table 1 are less than 25 W h kg^{-1}. The amount of electrolyte added to a coin or Swagelok-type cells is rarely provided in the literature, it was assumed 85 μl of electrolyte will fill the 2032 coin cell space. In order to achieve a practical energy density of 500 W h kg^{-1}, the E/C ratio should be less than 1.5 g A h^{-1} at an areal capacity of 6 mA h cm^{-2} and a N/P ratio of 1.5 without a solid-state Li^+ conductor based on our simulation.[10] Therefore, it is very important to quantify the TEGDME decomposition to develop more stable solvents, which enable to decrease E/C ratio further (a lean electrolyte condition).

The main feature in Fig. 2b is a flat plateau at 2.7 V on discharge (after correcting the *iR* loss by the solid-state Li^+ conductor as discussed below) after the first cycle and a gradual increase during the second half of the charge cycle, which is a combined result from both by-product accumulation and its insulating nature. It is noteworthy that the discharge potential in the first cycle quickly drops rapidly at the start of discharge, whereas those in subsequent cycles becomes more gradual. The discharge potential changes little from the second cycle,

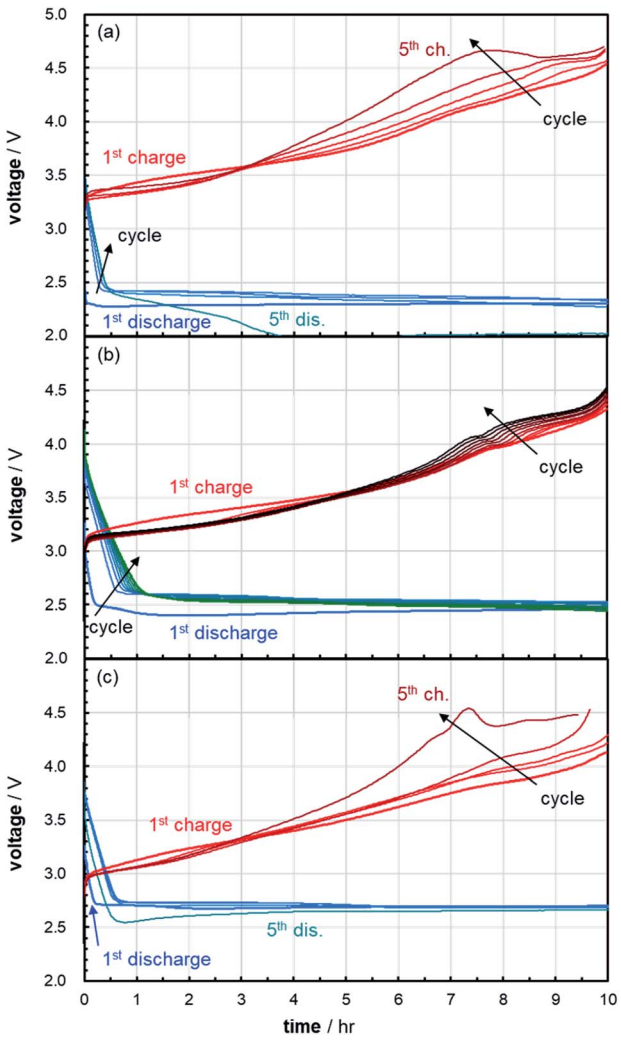

Fig. 2 Discharge/charge curves of the Li–O_2 cells with 1 M LiTFSI/TEGDME under O_2 flow shown in Fig. 1. Discharge/charge current densities are (a) 0.4 mA cm^{-2}, (b) 0.2 mA cm^{-2}, and (c) 0.2 mA cm^{-2}, without a solid-state Li^+ conductor in cell assembly.

 This journal is © The Royal Society of Chemistry 2020

Open Access Article. Published on 07 December 2020. Downloaded on 2/23/2026 11:56:04 AM.
This article is licensed under a Creative Commons Attribution-NonCommercial 3.0 Unported Licence.

however, the charge potential during subsequent cycles changes significantly. The same experiment without the solid-state Li^+ conductor was conducted to know its effect as shown in Fig. 2c, where only 5 cycles were obtained. The existence of the solid-state Li^+ conductor enhanced the cycle life by removing a factor of the parasitic reactions with Li metal negative electrode, although about 1 V/mA cm^{-2} polarization (*iR* loss) was imposed both for discharge and charge potentials by the 180 μm thick solid-state Li^+ conductor.

Investigation of parasitic reactions in the porous carbon positive electrode

Operando on-line gas chromatography analysis with a thermal conductivity detector was carried out to examine evolved gases on discharge and charge at a current density of 0.2 mA cm^{-2}. Little gas evolution was detected during discharge, and the evolutions of H_2O and CO_2 were observed during charge as shown in Fig. 3. These results indicate that TEGDME decomposition to produce gas components is very small during discharge as far as the discharge potential was maintained over 2 V. We have clearly observed the gradual increase of H_2O during charge and its gradual decrease during discharge. It is evident that CO_2 is generated at the final stage of charge, when the potential reached about 4 V. It is considered that H_2O is reproduced during charge by the oxidation of TEGDME and/or its organic fragments with the accumulation of carboxylate and carbonate species, which are eventually converted to CO_2 at higher potentials. The produced Li_2CO_3, which is called as Achilles' heel of lithium-air batteries,[32] can be electrochemically decomposed to CO_2 (eqn (6)), however, it cannot be completely removed and is accumulated over repeated cycles, which results in the overpotential increase and the poor rechargeability.

$$2Li_2CO_3 \rightarrow 2CO_2 + O_2 + 4Li^+ + 4e^- \quad (6)$$

To make a quantitative analysis of H_2O and CO_2 during charge, on-line mass spectroscopy analysis was carried out. After discharge, the remaining O_2 in the cell was flushed out by switching the inlet gas to He, so that the evolved gases during charge can be analyzed. Again, we have observed negligible H_2O formation during discharge under O_2 atmosphere and gradual increase of H_2O during charge under He atmosphere as shown in Fig. 4. The evolution of H_2O and CO_2 started from about 3.1 and 3.7 V (after correcting *iR* loss) on the first charge, respectively. Almost the same curves were reproduced at 0.4 mA cm^{-2} as shown in Fig. 5a. By using isotope labeled $^{18}O_2$ (purity ≥ 98%), it was proved that the oxygen atom in H_2O and CO_2 are mainly originated from introduced O_2 during discharge as shown in Fig. 5b. However, the evolution of the scrambled $C^{16,18}O_2$ indicates that the oxygen atom partly comes from the solvent decomposition as reported before.[31] Since the behaviors of $C^{16,18}O_2$ and $C^{16}O_2$ seems different from that of $C^{18}O_2$ during 8 hours before the rapid CO_2 generation, it may contain a small amount of the organic fragments with m/z = 46 and 44 in $C^{16,18}O_2$ and $C^{16}O_2$ curves in Fig. 5b, respectively. Therefore, integrated CO_2 amount in Fig. 4 was corrected using the ratio $C^{18}O_2 : C^{16,18}O_2 : C^{16}O_2 = 61 : 35 : 4$.

The evolved O_2 was calculated to be 73% expected form the charge amount ($O_2/2e^-$ = 0.73) by integrating O_2 generation curve. The parasitic reactions to afford H_2O and CO_2 were calculated to be 7% and 8%, respectively. The remaining 12% of the charge amount was consumed for unknown by-products including incomplete yield of Li_2O_2 during discharge. On the third charge, the evolved O_2 decreased to 58% and the parasitic reactions to afford H_2O and CO_2 increased to 9% and 14%, respectively. The evolution of CO_2 started from about 3.5 V (after correcting *iR* loss) earlier than 3.7 V on the first charge.

The comparison in decay curves of H_2O between Fig. 3 (0.2 mA cm^{-2}, 2 ml min^{-1} O_2 flow) and Fig. 4 (0.2 mA cm^{-2}, 5 ml min^{-1} He flow) certainly proves the consumption of H_2O during discharge. This new observation might become possible using the two-compartment cell, because H_2O is lost by the reaction of Li metal negative electrode without the solid-state Li^+ conductor.

The reason why water is consumed during discharge is unclear at present. The possibility is a protonation of Li_2O_2 or

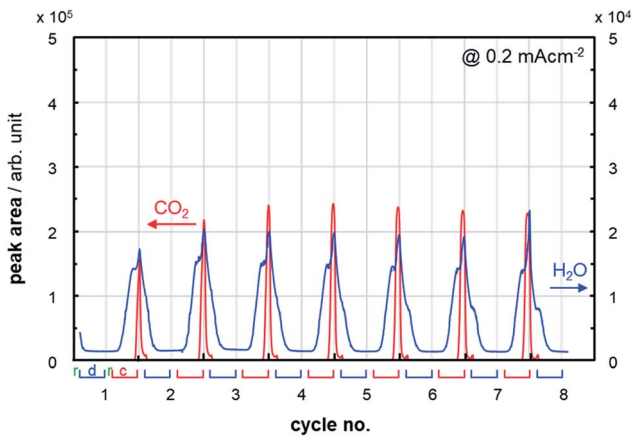

Fig. 3 On-line GC analysis during discharge/charge cycling of the Li–O_2 cell with 1 M LiTFSI/TEGDME under O_2 flow at 0.2 mA cm^{-2}. r, d, and c denote rest, discharge, and charge, respectively.

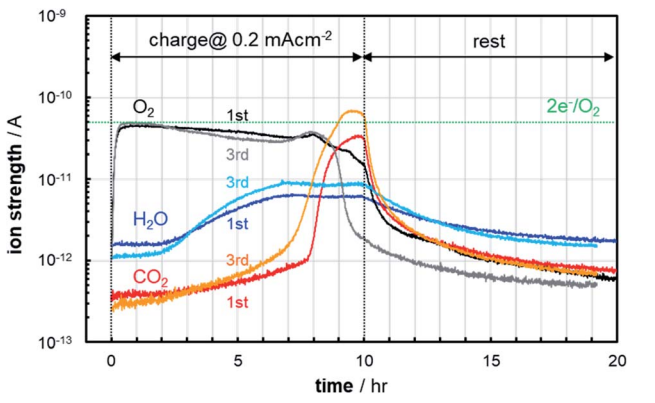

Fig. 4 On-line MS analysis of the Li–O_2 cell with 1 M LiTFSI/TEGDME during the first and the third charge at 0.2 mA cm^{-2} and the following rest under He atmosphere, after the first and the third discharge at 0.2 mA cm^{-2} under O_2 atmosphere.

Open Access Article. Published on 07 December 2020. Downloaded on 2/23/2026 11:56:04 AM.
This article is licensed under a Creative Commons Attribution-NonCommercial 3.0 Unported Licence.

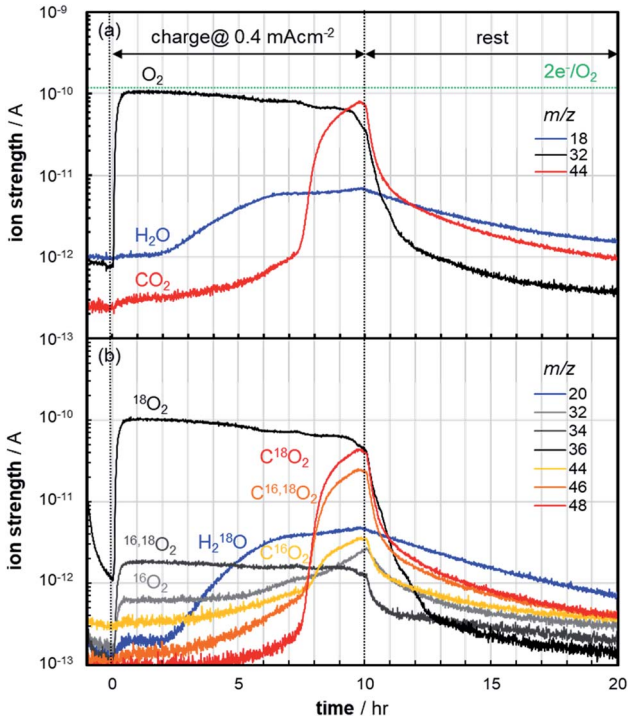

Fig. 5 On-line MS analysis of the Li–O_2 cell with 1 M LiTFSI/TEGDME during the first charge at 0.4 mA cm^{-2} and the following rest under He atmosphere, after the first discharge at 0.4 mA cm^{-2} under (a) $^{16}O_2$ and (b) $^{18}O_2$ atmosphere.

LiO_2 in eqn (7) and (8), respectively. However, these protonation by water is thermodynamically unfavorable due to the very high pK_a ($\approx$33) of water.[30,33] However, the quantitative reaction between the Li_2O_2 formed electrochemically on carbon electrodes and water (eqn (7)) was used for a photometric analysis (DIN 38409-15)[30] or an iodometric titration for H_2O_2.[34] Furthermore, if these reactions are followed by the disproportionation reaction, the net reactions (eqn (9) and (10)) become thermodynamically favorable.[33,35] Therefore, it is reasonable to consider that the water produced during charge reacts with the formed Li_2O_2 or LiO_2 during discharge, which might be one of the reasons for incomplete yield of Li_2O_2. The formation of LiOH has been reported,[23,36,37] and its constant accumulation in the carbon electrode is considered as one of reasons for the poor rechargeability. Because the removal of LiOH needs a little bit higher potential (4.5 V *vs.* Li/Li^+)[35] than that of Li_2CO_3 (4.3 V,[35] 3.8–4.2 V [38]). The water effect on the nonaqueous Li–O_2 technology is still ambiguous.[39]

$$Li_2O_2 + 2H_2O \rightarrow H_2O_2 + 2LiOH \quad (7)$$

$$LiO_2 + H_2O \rightarrow HO_2 + LiOH \quad (8)$$

$$2Li_2O_2 + 2H_2O \rightarrow 4LiOH + O_2 \quad (9)$$

$$2LiO_2 + H_2O \rightarrow LiOOH + LiOH + O_2 \quad (10)$$

The pressure change was monitored to provide the amounts of O_2 consumed during discharge and evolved during charge based on the ideal gas law. The results obtained from the closed cell could deviate from those obtained from the flow cell as cycled, because by-products accumulated inside the cell influence the reaction process. Therefore, we adopted the pressure measurement only for the first 2 cycles as shown in Fig. 6a. Fig. 6b shows the O_2 efficiency for discharge and charge. If the ideal reaction (eqn (4)) exclusively occurs, the O_2 efficiency (O_2/2e$^-$) should be 1 both for discharge and charge. The O_2 efficiency for the first discharge was 0.92, meaning O_2 consumption was 8% lower than the ideal, and hence, parasitic reactions other than Li_2O_2 formation occurred. In the similar way, the O_2 efficiency for the first charge was 0.77, meaning O_2 evolution was 23% lower than the ideal. This value deviates a little from that obtained by on-line MS analysis (0.73). These O_2 efficiencies for the first discharge and charge are relatively comparable with the data reported at different conditions (0.92 and 0.64, respectively).[22]

We have observed a short plateau at the very beginning of the second discharge as shown in Fig. 6a, where some electrochemical reaction without O_2 consumption occurred. This parasitic reaction accounted for 7% of the discharge amount, and it gradually increased as cycled.

The results summarized in Table 2 clearly show parasitic reactions to unknown by-products increased drastically as cycled. The O_2 efficiency for the third discharge was obtained by the same pressure measurement, where the gas phase was purged out by O_2 at 5 ml min^{-1} for 30 min after the second cycle. The total electric charge consumed for parasitic reactions were 35 and 59% at the first and the third cycle, respectively.

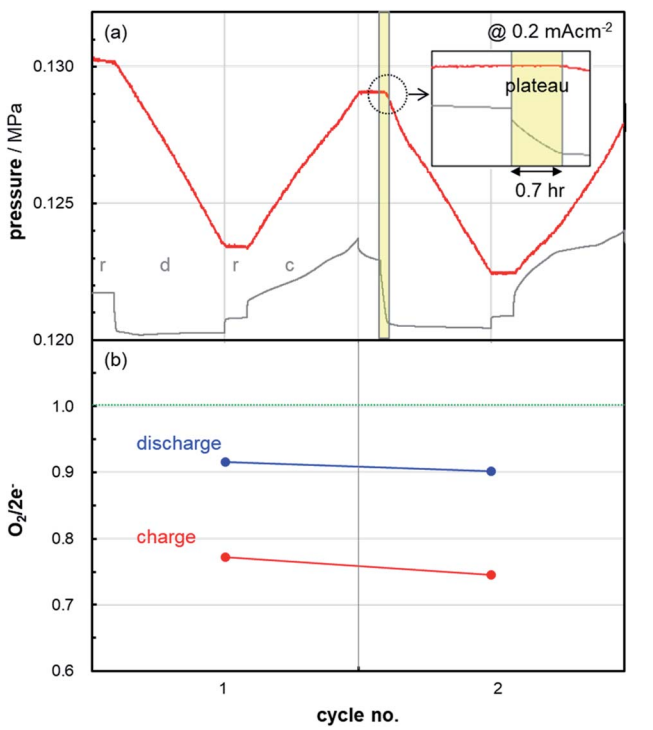

Fig. 6 The change of (a) pressure and (b) O_2 efficiency of the Li–O_2 cell with 1 M LiTFSI/TEGDME during cycles at 0.2 mA cm^{-2}. Potential profile is added as a dimmed line for reference.

This journal is © The Royal Society of Chemistry 2020

Open Access Article. Published on 07 December 2020. Downloaded on 2/23/2026 11:56:04 AM.
This article is licensed under a Creative Commons Attribution-NonCommercial 3.0 Unported Licence.

Table 2 Material balance of electrochemical reactions in the Li–O_2 cell with 1 M LiTFSI/TEGDME at 0.2 mA cm^{-2}

	Discharge (ORR)			Charge (OER)				
Cycle no.	Li_2O_2 formation	Unknown w/o O_2	Unknown w/O_2	Unknown w/o O_2	O_2 evolution	H_2O evolution	CO_2 evolution	Li_2O_2 loss
1	92	0	8	8	73	7	8	4
3	83	7	10	17	58	9	14	2

Mechanism of TEGDME decomposition

To know the decomposition reactions of TEGDME, the decomposition products in gas phase were collected every one hour during discharge/charge and characterized by GC/MS equipped with a thermal separation probe. Fig. 7a is an example chart obtained during the third charge (final one hour). Major by-products were ethylene glycol methyl ether (2-methoxyethanol), ethylene glycol methyl methoxymethyl ether and an unidentified alcohol in addition to smaller glymes, $CH_3O(CH_2CH_2O)_nCH_3$ (n = 1–3). Fig. 7b, c and d show their distribution change every one hour during the first discharge, the first charge and the third charge, respectively. The major by-products continued to grow particularly during charge. A small amount of aldehyde and vinyl ether were also detected, which behaved differently with the major by-products due to their unstable nature.

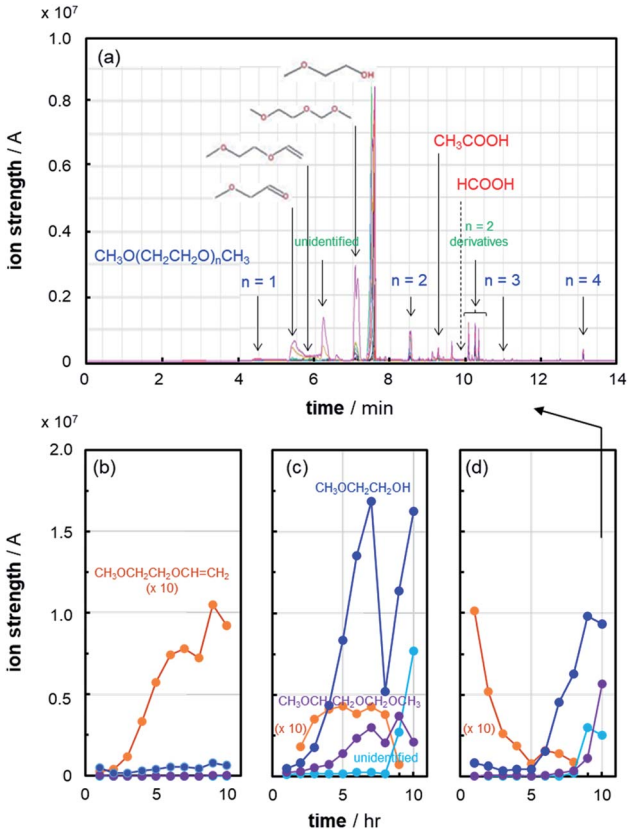

Fig. 7 (a) TSP-GC/MS analysis for by-products derived from TEGDME during the third charge (final one hour), and their distribution change during (b) the first discharge, (c) the first charge and (d) the third charge.

The decomposition products in liquid phase were also analyzed by LC/MS. We have observed gradual increase of methylene oxide chain derivatives, $CH_3O(CH_2CH_2O)_p(CH_2O)(CH_2CH_2O)_qCH_3$ ($p, q \geq 0, p + q$ = 2–5) as well as larger glymes (n = 5, 6) during 5 cycles as shown in Fig. 8.

Based on the observed by-products, possible mechanism for the TEGDME decomposition is proposed in Fig. 9. The decomposition of TEGDME (**1**) can be initiated by hydrogen atom abstraction by singlet oxygen ($^1O_2$) or superoxide radical anion ($O_2^{\bullet -}$). Because the stability of alkyl radicals is in the order of tertiary > secondary > primary, hydrogen atoms on ethylene groups (**3**) are susceptible to hydrogen abstraction than those on terminal methyl groups (**2**) as was reported for ethylene glycol dimethyl ether (monoglyme).[40] The radical thus formed (**3**) may undergo β-scission (C–O scission) to give other radicals (**5**, **4′**) and unsaturated fragments (**6**, **7**).[41] Actually, unsaturated compounds (**6**; m = 1, and **7**; m = 0) were detected. The resultant radicals (**4′**, **5′**) may undergo recombination by radical coupling to generate various glymes (**1′**) comprising from monoglyme (n = 1), diglyme (n = 2), triglyme (n = 3), and other oligomers, which were detected up to n = 6 after 5 cycles. The hydrogen abstraction from terminal methyl groups (**2**) also seems to happen,[41] because various methylene oxide chain derivatives (**8**; $p + q$ = 2–5) were detected, which can be formed by the similar radical coupling (**2′**, **5′**). Then, the same reactions are repeated for various glymes (**1′**) and methylene oxide chain derivatives (**8**) to produce a variety of homologues.

Besides the decomposition mechanism proposed for monoglyme,[40,42,43] we would like to point out that formate esters (**9**) might be produced by the $^{\bullet}$OH radical initiated oxidation of

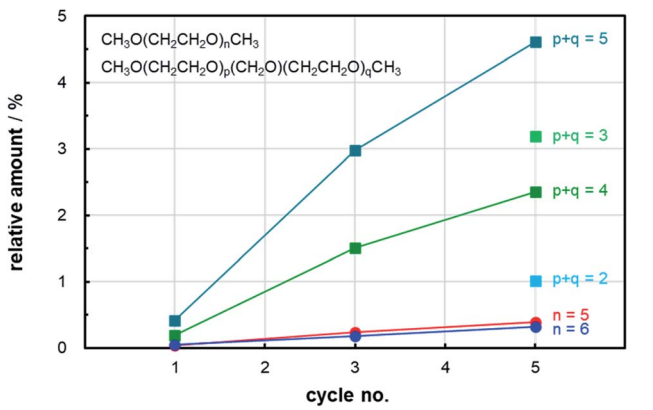

Fig. 8 LC/MS analysis for by-products derived from TEGDME after 5 cycles. Relative amount against TEGDME.

Open Access Article. Published on 07 December 2020. Downloaded on 2/23/2026 11:56:04 AM.
This article is licensed under a Creative Commons Attribution-NonCommercial 3.0 Unported Licence.

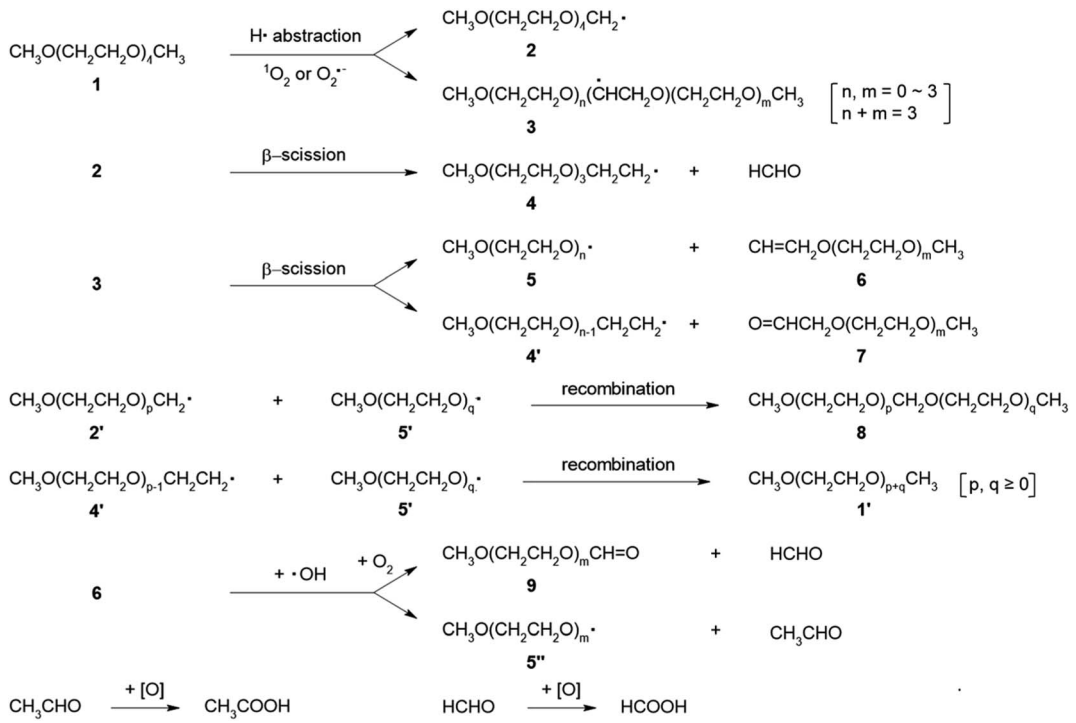

Fig. 9 Possible mechanisms for TEGDME decomposition.

vinyl ethers (**6**),[44] where ·OH radicals can be generated by singlet oxygen and water.[45] The degradation reactions of the aldehydes (**7**) leading to formic/acetic acids (or formate/acetate) are complex to describe. Any alkyl radicals (**2**, **3**, **4**) can lead to ether peroxides, which readily undergo oxidative decomposition analogous to combustion reactions.

The decomposition reactions shown in Fig. 9 are possible both for discharge and charge. H_2O is generated from about 3.1 V (after correcting *iR* loss) by electrochemical oxidation of organic fragments, and accumulated formate/acetate is electrochemically oxidized from about 3.5 V (after correcting *iR* loss) to generate CO_2 during charge according to eqn (11).[46] The H_2O accompanied during charge is successively accumulated, which can alter the reaction process as represented in eqn (9) and (10), and also cause the hydrolysis of glymes and other organic intermediates. It is considered that ethylene glycol methyl ether and the unidentified alcohol can be produced by hydrolysis. Li_2CO_3 can be formed by not only the mirror process of eqn (6), but also eqn (12).

$$RCOO^- \rightarrow CO_2 + R^{\cdot} + e^- \ (R = H, CH_3) \quad (11)$$

$$2LiOH + CO_2 \rightarrow Li_2CO_3 + H_2O \quad (12)$$

We have successfully envisaged the material balance of the Li–O_2 cell with 1 M LiTFSI/TEGDME at 0.2 mA cm^{-2} as listed in Table 2. 8% of the discharge amount was assigned for parasitic reactions other than Li_2O_2 formation during the first discharge, which can be attributed to the reaction between ($^1O_2$ and/or $O_2^{\cdot -}$) and (TEGDME and/or its fragments in Fig. 9). On the other hand, 8% of the charge amount was assigned for parasitic reactions other than gas evolution, which can be attributed to the reaction between ($^1O_2$ and/or $O_2^{\cdot -}$) and (TEGDME and/or its fragments in Fig. 9) including the electrochemical oxidation of by-products during the first discharge. 4% of the charge amount can be assigned to the loss of Li_2O_2, probably through LiOH formation discussed before. The parasitic reactions without O_2 consumption at the very beginning of the discharge from the second cycle can be attributed to the electrochemical reduction of the oxidized moieties during charge.

Effect of redox mediators

The electrolyte decomposition passivates the surface of the carbon electrode and Li_2O_2, which increases the overpotential

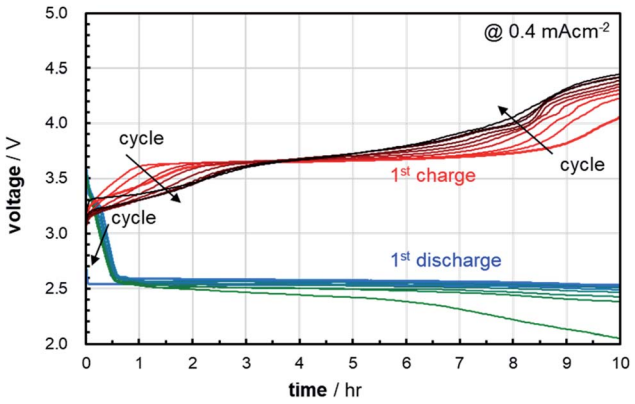

Fig. 10 Discharge/charge curves of the Li–O_2 cells with 0.5 M LiTFSI + 0.5 M $LiNO_3$ + 0.2 M LiBr/TEGDME under O_2 flow at 0.4 mA cm^{-2}.

This journal is © The Royal Society of Chemistry 2020

Open Access Article. Published on 07 December 2020. Downloaded on 2/23/2026 11:56:04 AM.
This article is licensed under a Creative Commons Attribution-NonCommercial 3.0 Unported Licence.

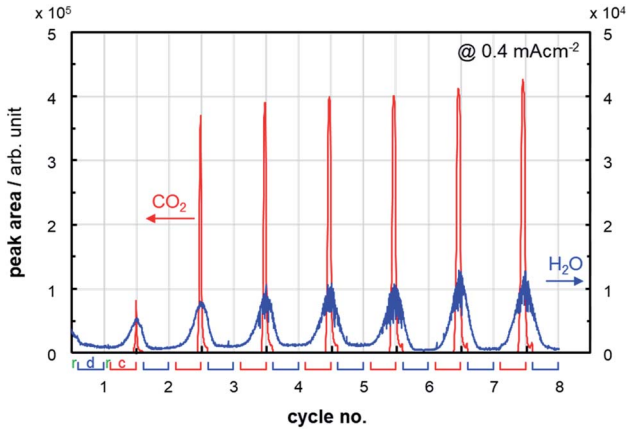

Fig. 11 On-line GC analysis during discharge/charge cycling of the Li–O_2 cell with 0.5 M LiTFSI + 0.5 M $LiNO_3$ + 0.2 M LiBr/TEGDME under O_2 flow at 0.4 mA cm^{-2}. r, d, and c denote rest, discharge, and charge, respectively.

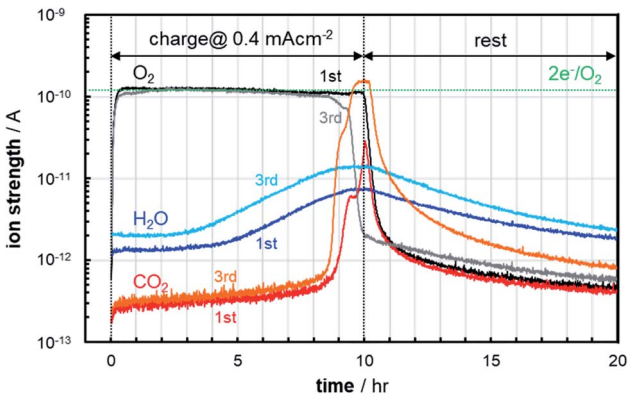

Fig. 12 On-line MS analysis of the Li–O_2 cell with 0.5 M LiTFSI + 0.5 M $LiNO_3$ + 0.2 M LiBr/TEGDME during the first and the third charge at 0.4 mA cm^{-2} and the following rest under He atmosphere, after the discharge at 0.4 mA cm^{-2} under O_2 atmosphere.

during cycling. Particularly, high polarization during charge beyond about 4 V deteriorates the cell. Redox mediators (RMs) have been proved to be useful at lowering charge potentials.[47] They are reversible redox couples which travels between the carbon electrode and Li_2O_2 surface and can oxidize Li_2O_2 through a chemical reaction instead of electrochemical oxidation as shown in eqn (13) and (14).

$$2RM^- \rightarrow 2RM + 2e^- \quad (13)$$

$$2RM + Li_2O_2 \rightarrow 2RM^- + 2Li^+ + O_2 \quad (14)$$

We have used 0.5 M LiTFSI + 0.5 M $LiNO_3$ + 0.2 M LiBr/TEGDME electrolyte, where $LiNO_3$ and LiBr are considered to function as $RM^-/RM = NO_2^-/NO_2$ starting from 3.6 V [48] and $(3Br^-)/Br_3^-$ from 3.5 V *vs.* Li/Li^+,[49] respectively. Fig. 10 shows the discharge/charge curves at 0.4 mA cm^{-2} for the first 10 cycles. A flat charge plateau was observed at 3.5 V (after correcting *iR* loss, 90 μm thick solid-state Li^+ conductor). This potential is ascribed to the redox potential of electrochemical oxidation of Br^- to Br_3^-. The initial shoulder in the subsequent discharge cycles is attributed to the electrochemical reduction of Br_3^- to Br^-, which gradually decreases as cycled. The charge potential during the first half of the subsequent charge cycles also gradually decreases, which is an indication of the different chemical process other than these redox mediators, approaching the behavior of 1 M LiTFSI/TEGDME. Owing to the suppression of the oxidative decomposition of TEGDME and/or its fragments, the cycle life was extended to 15 cycles at 0.4 mA cm^{-2}.

Irrespective of the presence of redox mediators, the same behavior was observed for H_2O and CO_2 by *operando* on-line gas chromatography analysis as shown in Fig. 11. We have observed again the gradual increase of H_2O during charge and its gradual decrease during discharge. On-line mass spectroscopy analysis in Fig. 12 revealed that the evolved O_2 was improved to 88% expected form the charge amount ($O_2/2e^- = 0.88$). The parasitic reactions to afford H_2O and CO_2 were dramatically decreased to 3% and 1%, respectively. The remaining 8% of the charge amount was consumed for unknown by-products including incomplete yield of Li_2O_2 during discharge. The evolution of H_2O and CO_2 started from about 3.4 V and 3.6 V (after correcting *iR* loss) on the first charge, respectively. On the third charge, the evolved O_2 decreased to 77% and the parasitic reactions to afford H_2O and CO_2 increased to 5% and 9%, respectively. The evolution of CO_2 started at almost the same potential with that on the first charge.

The O_2 efficiency calculated from the pressure change for the first discharge was remarkably improved to 0.96 ($O_2/2e^- = 0.96$). A short plateau at the very beginning of the second discharges corresponds to 6% of the discharge amount, where some electrochemical reactions without O_2 consumption occurred.

The results summarized in Table 3 clearly show the suppression of parasitic reactions by the utilization of redox

Table 3 Material balance of electrochemical reactions in the Li–O_2 cell with 0.5 M LiTFSI + 0.5 M $LiNO_3$ + 0.2 M LiBr/TEGDME at 0.4 mA cm^{-2}

	Discharge (ORR)			Charge (OER)				
Cycle no.	Li_2O_2 formation	Unknown w/o O_2	Unknown w/O_2	Unknown w/o O_2	O_2 evolution	H_2O evolution	CO_2 evolution	Li_2O_2 loss
1	96	0	4	4	88	3	1	4
3	93	6	1	7	77	5	9	2[a]

[a] Estimation.

Open Access Article. Published on 07 December 2020. Downloaded on 2/23/2026 11:56:04 AM.
This article is licensed under a Creative Commons Attribution-NonCommercial 3.0 Unported Licence.

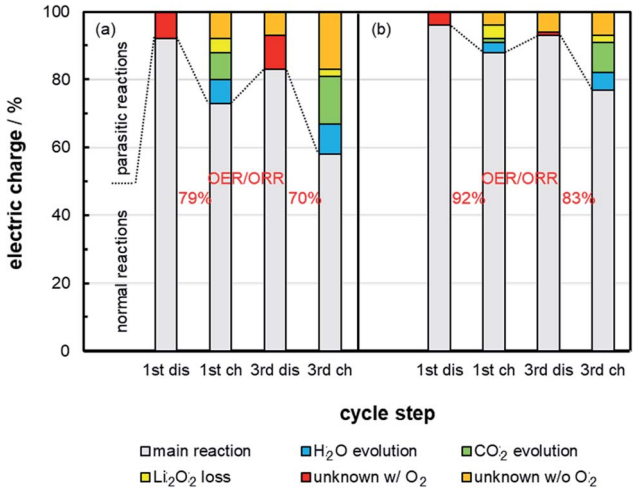

Fig. 13 The balance of total electric charge for the Li–O_2 cells with (a) 1 M LiTFSI/TEGDME at 0.2 mA cm^{-2}, and (b) 0.5 M LiTFSI + 0.5 M $LiNO_3$ + 0.2 M LiBr/TEGDME at 0.4 mA cm^{-2}.

mediators. The yield of Li_2O_2 for the third discharge was estimated from the assumption that a side reaction with Li_2O_2 loss is the same as 1 M LiTFSI/TEGDME system. The total electric charge consumed for parasitic reactions were 16 and 30% at the first and the third cycle, respectively.

Correlation between TEGDME decomposition and cycle life

To compare the two electrolyte systems, the results in Tables 2 and 3 were summarized in Fig. 13. The CE is often reported as an indicator of the efficiency of Li metal deposition and stripping, because it is a critical factor to predict the cycle life of Li metal batteries.[50] In the case of O_2 electrodes, OER/ORR is used as a rechargeability index. The (OER/ORR)s for the first and the third cycles were 79 and 70% for (a) 1 M LiTFSI/TEGDME at 0.2 mA cm^{-2}, and 92 and 83% for (b) 0.5 M LiTFSI + 0.5 M $LiNO_3$ + 0.2 M LiBr/TEGDME at 0.4 mA cm^{-2}, respectively. The changes from the first cycle to the third cycle were 9% decrease for both (a) and (b). If we apply the methodology of Li electrode, the cycle life at half capacity retention is forecasted to be 15 by $(1–0.09/2)^{15} \approx 0.5$, which is comparable with our experimental results (18 and 15 cycles).

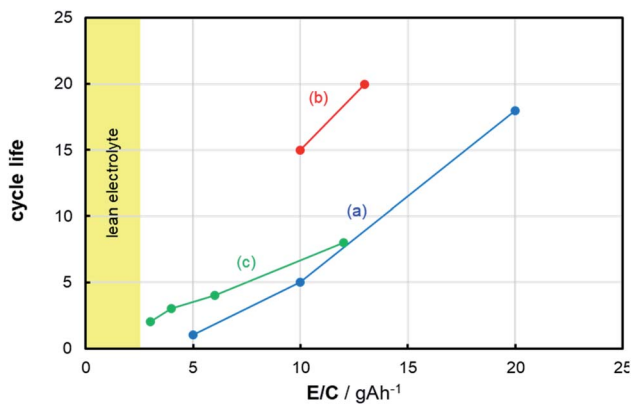

Fig. 14 Correlation between electrolyte amount (E/C) and cycle life; (a) 1 M LiTFSI/TEGDME at 0.8, 0.4, 0.2 mA cm^{-2}, (b) 0.5 M LiTFSI + 0.5 M $LiNO_3$ + 0.2 M LiBr/TEGDME at 0.4 mA cm^{-2}, (c) ref. 13 at 0.15 mA cm^{-2}.

Average TEGDME consumption rates from the second cycle to the fifth cycle were about 0.15 and 0.09 g A h^{-1} for (a) 1 M LiTFSI/TEGDME at 0.2 mA cm^{-2} and (b) 0.5 M LiTFSI + 0.5 M $LiNO_3$ + 0.2 M LiBr/TEGDME at 0.4 mA cm^{-2}, respectively. Thus, dry-up of electrolytes is expected to be after 133 and 111 cycles, respectively, which are far from the observed cycle life (18 and 15 cycles). The cause of the early failure is the by-product accumulation in the carbon electrode, which results in large potential polarization including deficient O_2 and Li^+ by pore clogging. This pore clogging was confirmed by a scanning electron microscope, Fourier transform infrared spectroscopy and impedance spectroscopy in Fig. S2–S4 given in the ESI.† This behavior in the O_2 electrode is similar to the case, when the cycle life is limited by the cell polarization due to the continuous irreversible electrolyte consumption forming a mossy SEI layer on the Li metal electrode of Li/$LiNi_{0.6}Co_{0.2}Mn_{0.2}O_2$ cells.[51] Fig. 14 shows a correlation between E/C and cycle life, although the cited data from ref. 13 include some influence from Li electrode. It is apparent that the E/C ratio is a good parameter to correlate with the cycle life at less electrolyte amount condition.

Although the utilization of redox mediators enabled to increase 2 times magnitude in the discharge/charge current density (*i.e.* areal capacity) while keeping a similar cycle life, it is still far to achieve satisfactory cycle life due to the short life of the redox mediators. Therefore, it is mandatory to find much more stable solvent against reactive oxygen species, which enables to operate under a lean electrolyte condition depicted as a yellow region in Fig. 14.

Conclusions

The material balance of the reactions occurring in the O_2 electrode of a Li–O_2 cell was examined, where a Ketjenblack-based porous carbon electrode comes into contact with a TEGDME-based electrolyte under more practical conditions of less electrolyte amount and high areal capacity. A custom-made two-compartment test cell was used, where anode and cathode compartments were separated by a solid-state Li^+ conductor to eliminate possible interference from the reactions at Li metal negative electrode. It was proved that the electrolyte amount is a major factor to limit the cycle life, and the ratio of electrolyte weight to cell capacity (E/C, g A h^{-1}) is a good parameter to correlate with the cycle life. Based on the by-product distribution, possible mechanism for TEGDME decomposition was proposed. Although these parasitic reactions were suppressed by the utilization of redox mediators, the cycle life was still only 15 cycles at a condition giving the energy density of 170 W h kg^{-1} for a complete cell level. Therefore, it is mandatory to find much more stable solvent against reactive oxygen species to achieve the targets of 'beyond LIB' even for low power application such as HAPS.

Furthermore, we obtained the following new information about the decomposition of TEGDME. (1) Produced H_2O is consumed during discharge, presumably by the reaction with

 This journal is © The Royal Society of Chemistry 2020

Open Access Article. Published on 07 December 2020. Downloaded on 2/23/2026 11:56:04 AM.
This article is licensed under a Creative Commons Attribution-NonCommercial 3.0 Unported Licence.

Li_2O_2 and/or LiO_2. (2) $CH_3O(CH_2CH_2O)_nCH_3$ and $CH_3O(CH_2CH_2O)_p(CH_2O)(CH_2CH_2O)_qCH_3$ are produced by radical recombination, which undergo repeated hydrogen atom abstraction by $^1O_2$ and/or $O_2^{\bullet-}$ similar with TEGDME. This ether regeneration mechanism might consume more electric amounts to show the lower O_2 efficiency but relatively tough cycle life.

Conflicts of interest

There are no conflicts to declare.

Acknowledgements

The present work was partially supported by the MEXT (Ministry of Education, Culture, Sports, Science and Technology) Program for the Development of Environmental Technology using Nanotechnology, and the ALCA-SPRING (Advanced Low Carbon Technology Research and Development Program – Specially Promoted Research for Innovative Next Generation Batteries) Project of the Japan Science and Technology Agency (JST). A part of this work was carried out at the SoftBank-NIMS Advanced Technologies Development Center as a joint research between NIMS and SoftBank Corp. Mass measurements were performed at the NIMS Battery Research Platform.

Notes and references

1 M. Winter, B. Barnett and K. Xu, Before Li ion batteries, *Chem. Rev.*, 2018, **118**, 11433–11456.
2 M. Li, J. Lu, Z. Chen and K. Amine, 30 years of lithium-ion batteries, *Adv. Mater.*, 2018, **30**, 1800561.
3 M. Ue and K. Uosaki, Recent progress in liquid electrolytes for lithium metal batteries, *Curr. Opin. Electrochem.*, 2019, **17**, 106–113.
4 K. M. Abraham and Z. Jiang, A polymer electrolyte-based rechargeable lithium/oxygen battery, *J. Electrochem. Soc.*, 1996, **143**, 1–5.
5 P. Bauer, High-energy-density systems, *Batteries for space power systems*, NASA, 1968, pp. 197–216.
6 H. Lee, D. J. Lee, M. Kim, H. Kim, Y. S. Cho, H. J. Kwon, H. C. Lee, C. R. Park and D. Im, High-energy density Li-O_2 battery with a polymer electrolyte-coated CNT electrode via the layer-by-layer method, *ACS Appl. Mater. Interfaces*, 2020, **12**, 17385–17395.
7 J. O. Park, M. Kim, J.-H. Kim, K. H. Choi, H. C. Lee, W. Choi, S. B. Ma and D. Im, A 1000 W h kg^{-1} Li-air battery: cell design and performance, *J. Power Sources*, 2019, **419**, 112–118.
8 K. Virwani, Y. Ansari, K. Nguyen, F. J. A. Moreno-Ortiz, J. Kim, M. J. Giammona, H.-C. Kim and Y.-H. La, In situ AFM visualization of Li-O_2 battery discharge products during redox cycling in an atmospherically controlled sample cell, *Beilstein J. Nanotechnol.*, 2019, **10**, 930–940.
9 K. Takechi, N. Singh, T. S. Arthur and F. Mizuno, Decoupling energy storage from electrochemical reactions in Li-air batteries toward achieving continuous discharge, *ACS Energy Lett.*, 2017, **2**, 694–699.
10 M. Ue, K. Sakaushi and K. Uosaki, Basic knowledge in battery research bridging the gap between academia and industry, *Mater. Horiz.*, 2020, **7**, 1937–1954.
11 W.-J. Kwak, R. Sharma, D. Sharon, C. Xia, H. Kim, L. R. Johnson, P. G. Bruce, L. F. Nazar, Y.-K. Sun, A. A. Frimer, M. Noked, S. A. Freunberger and D. Aurbach, Lithium-oxygen batteries and related systems: potential, status, and future, *Chem. Rev.*, 2020, **120**, 6626–6683.
12 T. Liu, J. P. Vivek, E. W. Zhao, J. Lei, N. Garcia-Araez and C. P. Grey, Current challenges and routes forward for nonaqueous lithium-air batteries, *Chem. Rev.*, 2020, **120**, 6558–6625.
13 S. Zhao, L. Zhang, G. Zhang, H. Sun and J. Yang, Failure analysis of pouch-type Li-O_2 batteries with superior energy density, *J. Energy Chem.*, 2020, **45**, 74–82.
14 J. Lai, Y. Xing, N. Chen, L. Li, F. Wu and R. Chen, Electrolytes for rechargeable lithium-air batteries, *Angew. Chem., Int. Ed.*, 2020, **59**, 2974–2997.
15 S. Feng, M. Chen, L. Giordano, M. Huang, W. Zhang, C. V. Amanchukwu, R. Anandakathir, Y. Shao-Horn and J. A. Johnson, Mapping a stable solvent structure landscape for aprotic Li-air battery organic electrolytes, *J. Mater. Chem. A*, 2017, **5**, 23987–23998.
16 M. Tang, J.-C. Chang, S. R. Kumar and S. J. Lue, Glyme-based electrolyte formulation analysis in aprotic lithium-oxygen battery and its cyclic stability, *Energy*, 2019, **187**, 115926.
17 J. Chen, C. Chen, T. Huang and A. Yu, LiTFSI concentration optimization in TEGDME solvent for lithium-oxygen batteries, *ACS Omega*, 2019, **4**, 20708–20714.
18 L. Carbone, P. T. Moro, M. Gobet, S. Munoz, M. Devany, S. G. Greenbaum and J. Hassoun, Enhanced lithium oxygen battery using a glyme electrolyte and carbon nanotubes, *ACS Appl. Mater. Interfaces*, 2018, **10**, 16367–16375.
19 A. Chamaani, M. Safa, N. Chawla, M. Herndon and B. El-Zahab, Stabilizing effect of ion complex formation in lithium-oxygen battery electrolytes, *J. Electroanal. Chem.*, 2018, **815**, 143–150.
20 M. Saito, T. Fujinami, S. Yamada, T. Ishikawa, H. Otsuka, K. Ito and Y. Kubo, Effects of Li salt anions and O_2 gas on Li dissolution/deposition behavior at Li metal negative electrode for non-aqueous Li-air batteries, *J. Electrochem. Soc.*, 2017, **164**, A2872–A2880.
21 C. Wu, T. Li, C. Liao, Q. Xu, Y. Cao, L. Li and J. Yang, Enhanced electrochemical performance of non-aqueous Li-O_2 batteries with triethylene glycol dimethyl ether-based electrolyte, *J. Electrochem. Soc.*, 2017, **164**, A1321–A1327.
22 D. W. Kim, S. M. Ahn, J. Kang, J. Suk, H. K. Kim and Y. Kang, In situ real-time and quantitative investigation on the stability of non-aqueous lithium oxygen battery electrolytes, *J. Mater. Chem. A*, 2016, **4**, 6332–6341.
23 M. Augustin, P. E. Vullum, F. Vullum-Bruer and A. M. Svensson, Inside the electrode: looking at cycling products in Li/O_2 batteries, *J. Power Sources*, 2019, **414**, 130–140.
24 E. Mourad, Y. K. Petit, R. Spezia, A. Samojlov, F. F. Summa, C. Prehal, C. Leypold, N. Mahne, C. Slugovc, O. Fontaine, S. Brutti and S. A. Freunberger, Singlet oxygen from cation driven superoxide disproportionation and consequences

Open Access Article. Published on 07 December 2020. Downloaded on 2/23/2026 11:56:04 AM.
This article is licensed under a Creative Commons Attribution-NonCommercial 3.0 Unported Licence.

for aprotic metal-O_2 batteries, *Energy Environ. Sci.*, 2019, **12**, 2559–2568.

25 S. A. Freunberger, Y. Chen, N. E. Drewett, L. J. Hardwick, F. Barde and P. G. Bruce, The lithium-oxygen battery with ether-based electrolytes, *Angew. Chem., Int. Ed.*, 2011, **50**, 8609–8613.

26 M. Marinaro, S. Theil, L. Jörissen and M. Wohlfahrt-Mehrens, New insights about the stability of lithium bis(trifluoromethane)sulfonimide-tetraglyme as electrolyte for Li-O_2 batteries, *Electrochim. Acta*, 2013, **108**, 795–800.

27 X. Bi, K. Amine and J. Lu, The importance of anode protection towards lithium oxygen batteries, *J. Mater. Chem. A*, 2020, **8**, 3563–3573.

28 F. Sun, R. Gao, D. Zhou, M. Osenberg, K. Dong, N. Kardjilov, A. Hilger, H. Markötter, P. M. Bieker, X. Liu and I. Manke, Revealing hidden facts of Li anode in cycled lithium-oxygen batteries through x-ray and neutron tomography, *ACS Energy Lett.*, 2019, **4**, 306–316.

29 H.-J. Shin, W.-J. Kwak, D. Aurbach and Y.-K. Sun, Large-scale Li-O_2 pouch type cells for practical evaluation and applications, *Adv. Funct. Mater.*, 2017, **27**, 1605500.

30 K. U. Schwenke, M. Metzger, T. Restle, M. Piana and H. A. Gasteiger, The influence of water and protons on Li_2O_2 crystal growth in aprotic Li-O_2 cells, *J. Electrochem. Soc.*, 2015, **162**, A573–A584.

31 B. D. McCloskey, D. S. Bethune, R. M. Shelby, G. Girishkumar and A. C. Luntz, Solvents' critical role in nonaqueous lithium-oxygen battery electrochemistry, *J. Phys. Chem. Lett.*, 2011, **2**, 1161–1166.

32 Z. Zhao, J. Huan and Z. Peng, Achilles' heel of lithium-air batteries: lithium carbonate, *Angew. Chem., Int. Ed.*, 2018, **57**, 3874–3886.

33 D. H. Chin, G. Chiericato, E. J. Nanni and D. T. Sawyer, Proton-induced disproportionation of superoxide ion in aprotic media, *J. Am. Chem. Soc.*, 1982, **104**, 1296–1299.

34 B. D. McCloskey, A. Valery, A. C. Luntz, S. R. Gowda, G. M. Wallraff, J. M. Garcia, T. Mori and L. E. Krupp, Combining accurate O_2 and Li_2O_2 assays to separate discharge and charge stability limitations in nonaqueous Li-O_2 batteries, *J. Phys. Chem. Lett.*, 2013, **4**, 2989–2993.

35 S. Meini, N. Tsiouvaras, K. UtaSchwenke, M. Piana, H. Beyer, L. Lange and H. A. Gasteiger, Rechargeability of Li-air cathodes pre-filled with discharge products using an ether-based electrolyte solution: implications for cycle-life of Li-air cells, *Phys. Chem. Chem. Phys.*, 2013, **15**, 11478–11493.

36 Z. Guo, X. Dong, S. Yuan, Y. Wang and Y. Xia, Humidity effect on electrochemical performance of Li-O_2 batteries, *J. Power Sources*, 2014, **264**, 1–7.

37 Z. Li, S. Ganapathy, Y. Xu, J. R. Hering, Q. Zhu, W. Chen and M. Wagemaker, Understanding the electrochemical formation and decomposition of Li_2O_2 and LiOH with operando X-ray diffraction, *Chem. Mater.*, 2017, **29**, 1577–1586.

38 N. Mahne, S. E. Renfrew, B. D. McCloskey and S. A. Freunberger, Electrochemical oxidation of lithium carbonate generates singlet oxygen, *Angew. Chem., Int. Ed.*, 2018, **57**, 5529–5533.

39 S. Ma, J. Wang, J. Huang, Z. Zhou and Z. Peng, Unveiling the complex effects of H_2O on discharge-recharge behaviors of aprotic lithium-O_2 batteries, *J. Phys. Chem. Lett.*, 2018, **9**, 3333–3339.

40 B. D. Adams, R. Black, Z. Williams, R. Fernandes, M. Cuisinier, E. J. Berg, P. Novak, G. K. Murphy and L. F. Nazar, Towards a stable organic electrolyte for the lithium oxygen battery, *Adv. Energy Mater.*, 2015, **5**, 1400867.

41 Y. Ogata, K. Takagi and T. Suzuki, Photolytic oxidation of ethylene glycol dimethyl ether and related compounds by aqueous hypochlorite, *J. Chem. Soc., Perkin Trans. 2*, 1978, **50**, 562–567.

42 Z. Huang, H. Zeng, M. Xie, X. Lin, Z. Huang, Y. Shen and Y. Huang, A stable lithium-oxygen battery electrolyte based on fully methylated cyclic ether, *Angew. Chem., Int. Ed.*, 2019, **58**, 2345–2349.

43 M. Carboni, A. G. Marrani, R. Spezia and S. Brutti, 1,2-Dimethoxyethane degradation thermodynamics in Li_2O_2 redox environments, *Chem.–Eur. J.*, 2016, **22**, 17188–17203.

44 G. Thiault, R. Thévenet, A. Mellouki and G. Le Bras, OH and O_3-initiated oxidation of ethyl vinyl ether, *Phys. Chem. Chem. Phys.*, 2002, **4**, 613–619.

45 X. Xu, R. P. Muller and W. A. Goddard, The gas phase reaction of singlet dioxygen with water: a water-catalyzed mechanism, *Proc. Natl. Acad. Sci. U. S. A.*, 2002, **99**, 3376–3381.

46 A. K. Vigh and B. E. Conway, Electrode kinetic aspects of the Kolbe reaction, *Chem. Rev.*, 1967, **67**, 623–664.

47 W. Zhao, X. Mu, P. He and H. Zhou, Advances and challenges for aprotic lithium-oxygen batteries using redox mediators, *Batteries Supercaps*, 2019, **2**, 803–819.

48 D. Sharon, D. Hirsberg, M. Afri, F. Chesneau, R. Lavi, A. A. Frimer, Y.-K. Sun and D. Aurbach, Catalytic behavior of lithium nitrate in Li-O_2 cells, *ACS Appl. Mater. Interfaces*, 2015, **7**, 16590–16600.

49 Z. Liang and Y.-C. Lu, Critical role of redox mediator in suppressing charging instabilities of lithium-oxygen batteries, *J. Am. Chem. Soc.*, 2016, **138**, 7574–7583.

50 B. D. Adams, J. Zheng, X. Ren, W. Xu and J.-G. Zhang, Accurate determination of coulombic efficiency for lithium metal anodes and lithium metal batteries, *Adv. Energy Mater.*, 2018, **8**, 1702097.

51 S. Chen, C. Niu, H. Lee, Q. Li, L. Yu, W. Xu, J.-G. Zhang, E. J. Dufek, M. S. Whittingham, S. Meng, J. Xiao and J. Liu, Critical parameters for evaluating coin cells and pouch cells of rechargeable Li-metal batteries, *Joule*, 2019, **3**, 1–12.

This journal is © The Royal Society of Chemistry 2020